Proceedings of ISERME 2025
19-20 September 2025
https://doi.org/10.31705/ISERME.2025.30

Development of a Digital Twin Construction Method for Abandoned and Closed Mines Contributing to Nature Positive

[*]Hamaguchi[1] R, Otsuka[1] N, Yasutaka[2,1] T, Yamagata[3] S, Kuroshima[3] S, Shingai[3] K, Okada[1] N, Ohtomo[1] Y and Kawamura[1] Y

[1]Faculty of Engineering, Hokkaido University, Sapporo, Japan

[2]National Institute of Advanced Industrial Science and Technology (AIST), Tsukuba, Japan

[3]Mitsubishi Materials Corporation, Tokyo, Japan

[*]Corresponding author – hamaguchi.reiko.w7@elms.hokudai.ac.jp

Abstract

The concept of Nature Positive (NP), which emphasizes the restoration of natural ecosystems, has gained increasing attention in recent years. In the context of closed mines, achieving a balance between the assessment and restoration of natural capital has become an urgent challenge. However, it has been difficult to maintain an accurate and continuous understanding of on-site conditions at these sites due to the extensive spatial scale of mine sites.

This study investigates the application of digital twin technology, which replicates physical environments in cyberspace, to support NP-aligned assessments of natural capital in closed mine management. The research focuses on tailings storage areas at a closed mine in Hokkaido, Japan, where aerial imagery acquired by drones was processed using Structure from Motion (SfM) to generate point cloud data and construct 3D models. Orthophotos were also produced through orthorectification. In addition, photorealistic images were rendered using 3D Gaussian Splatting, which enables free-viewpoint observation and supports the assessment of natural capital.

The results demonstrate the potential of these technologies as effective alternatives to conventional on-site visual inspections. By integrating 3D visualization and spatial data, this study establishes a technological foundation for the objective assessment of environmental conditions at closed mine sites, contributing to the realization of Nature Positive mining practices.

Keywords: 3D Gaussian Splatting, Environmental Monitoring, Structure from Motion, Vegetation Index

1 Introduction

Nature Positive (NP) is a globally recognized and increasingly important concept aimed at halting and reversing biodiversity loss [1]. In the context of managing abandoned and decommissioned mines, efforts to restore vegetation and ecosystems that were lost due to historical mining activities contribute directly to achieving NP goals. However, traditional environmental management of mines faces several challenges. Mine sites are often vast, located in remote areas, and can be dangerous to access for surveys. Furthermore, there is a growing need to streamline environmental management processes in the face of a shrinking workforce. To address these challenges, digital twin technology, which creates a virtual replica of a physical environment, has garnered significant attention. Digital twins enable real-time monitoring and prediction through bidirectional interaction between the physical and cyber spaces. This technology is being applied across various mining operations, including exploration, blasting, safety management, and environmental monitoring [2, 3]. However, the lack of on-site network systems

and the high cost of data acquisition present significant barriers to its wider adoption [3]. This study aims to build a foundational digital twin for an abandoned mine in Hokkaido, Japan, using aerial data captured by a drone. We utilized a drone equipped with RGB and multispectral cameras to capture images of the site. Structure from Motion (SfM) was then used to create 3D models and orthomosaics. We further applied 3D Gaussian Splatting (3DGS) technology to enable high-fidelity photorealistic rendering. Furthermore, we attempted to visualize vegetation conditions for NP initiatives using these digital twin technologies. Specifically, we sought to develop a custom Vegetation Index (VI). While the Normalized Difference Vegetation Index (NDVI) is commonly used to assess vegetation, it is susceptible to atmospheric and soil interference and its sensitivity decreases as vegetation density increases, making accurate evaluation difficult under specific environmental conditions [4]. Therefore, this study aims to design a unique VI tailored to the specific characteristics of the study area. This is to improve the visualization accuracy of vegetation health and diversity, which is difficult to represent with conventional indicators. Through this research, we aim to propose a digital twin-based method for implementing NP practices to support the natural restoration process at abandoned mine sites.

2 Methodology

2.1 Study Site

The study site was an abandoned mine (hereafter, Mine X) located in Hokkaido, Japan, with the investigation focusing on its tailings dump. The specific location details are withheld for anonymity. The study area was divided into two plots, each approximately 10m×10m in size: Area A, characterized by relatively open terrain (Figure 1a), and Area B, with dense vegetation (Figure 1b). The dominant plant species were trees such as Japanese white birch (*Betula platyphylla* var. *japonica*) and pine (*Pinus* spp.), as well as various herbaceous plants. Trees were sparsely distributed in Area A, which was dominated by low-lying herbaceous vegetation, while Area B had a high density of trees. The positional relationship between these areas is shown in Figure 2.

Figure 1a: Appearance of Area A

Figure 1b: Appearance of Area B

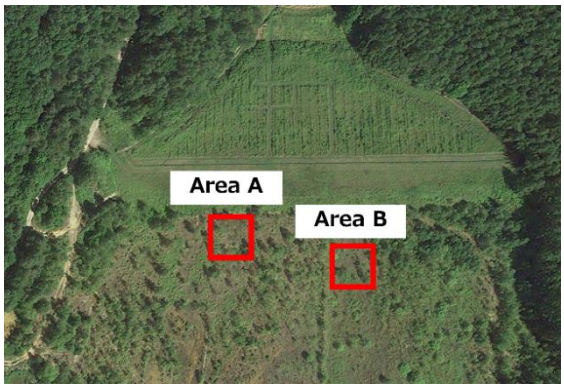

Figure 2: Location of Area A and Area B

2.2 Equipment and Data Acquisition Conditions

In this study, aerial imagery of the target site was acquired using a DJI Mavic 3 Thermal (hereafter referred to as *Mavic*) and a DJI Phantom 4 Multispectral (hereafter referred to as *Phantom*). The Mavic is equipped with both an RGB camera and a thermal infrared camera, enabling the simultaneous acquisition of visible and thermal imagery. In contrast, the Phantom is equipped with an RGB camera and a multispectral sensor consisting of five bands:

Blue, Green, Red, Near-Infrared (NIR), and Red Edge. The flight conditions are summarized in Table 1.

Table 1: Flight conditions of UAV-based data acquisition

Parameter	Mavic	Phantom
Date and time of flight	July 25, 2025, 10:00–11:00 JST	July 24, 2025, 14:00–15:00 JST
Weather conditions	Clear, 31 °C, 62% humidity, wind 2 m/s	Clear, 31 °C, 58% humidity, wind 3 m/s
Flight altitude	13m	12m
Flight speed	2.5m/s	3m/s
Front overlap	80%	85%
Side overlap	70%	75%

For both UAVs, flight routes were pre-programmed using DJI's proprietary applications (*DJI Pilot 2* for the Mavic and *DJI GS Pro* for the Phantom), and images were acquired through automated flight missions. Georeferencing was achieved via the onboard RTK (Real-Time Kinematic) positioning system, without the use of Ground Control Points (GCPs).

2.3 Structure-from-Motion (SfM)

Aerial images obtained from the UAV surveys were processed using **Agisoft Metashape Professional (v2.2.1)** to generate 3D models and orthophotos based on the Structure-from-Motion (SfM) approach. SfM is a photogrammetric technique that reconstructs three-dimensional structures (point clouds) of a target object by identifying corresponding features across multiple images captured from different viewpoints [5]. In this study, both RGB and multispectral datasets were processed. Specifically, photo alignment (camera pose estimation) and point cloud generation were performed. A Digital Elevation Model (DEM) was subsequently derived from the reconstructed point cloud, which was then used to produce orthomosaics. In addition, a 3D textured mesh was created separately using only RGB imagery. Thermal imagery was processed solely for orthophoto generation and was used for reference purposes.

2.4 3D Gaussian Splatting (3DGS) for Rendering

3D Gaussian Splatting (3DGS) is a novel rendering technique that represents three-dimensional structures by placing a large number of Gaussian ellipsoids (splats) in 3D space, based on images acquired from multiple viewpoints and their corresponding camera parameters [6]. Unlike conventional 3D models, which are typically constructed from point clouds or polygonal meshes, 3DGS provides a smoother spatial representation with high rendering speed and accuracy. Moreover, it eliminates the need for texture mapping or mesh reconstruction, thereby allowing complex scenes to be represented with enhanced visual realism. In this study, camera intrinsics and extrinsics, along with the RGB images reconstructed via Metashape, were exported in COLMAP format. These data were subsequently processed using **PostShot**, a software that imports COLMAP datasets and performs scene reconstruction and rendering by optimizing Gaussian splats in 3D space.

2.5 Vegetation Visualization Method

In this study, an exploratory search for a site-specific vegetation index (VI) was conducted using the orthomosaic of multispectral images generated through SfM. The most commonly applied index, the Normalized Difference Vegetation Index (NDVI), represents vegetation activity and is defined as:

$$NDVI = \frac{NIR - Red}{NIR + Red} \quad (1)$$

where **NIR** denotes the reflectance of the near-infrared band and **Red** the reflectance of the red band. NDVI exploits the spectral properties of vegetation, which absorbs red light during photosynthesis while strongly reflecting near-infrared radiation, yielding values ranging from −1 to 1 [4]. Higher NDVI values (closer to 1) indicate denser vegetation coverage.

In this study, a brute-force search was performed to identify novel indices using the reflectance of five bands (Blue, Green, Red, Red Edge, and NIR). The general form of the candidate equation was expressed as:

$$VI = \frac{f * Blue + g * Green + h * Red + i * RedEdge + j * NIR}{a * Blue + b * Green + c * Red + d * RedEdge + e * NIR} \quad (2)$$

where coefficients a, b, c, d, e, f, g, h, i, j take values from {−1, 0, 1}. Equation (2) follows the exhaustive search methodology proposed by Abe et al. (2023) [7] in the context of mineral and rock visualization. While their approach evaluated discrimination performance using masked samples of minerals and rocks, direct application to the present study was not feasible, as vegetation types in the study area were not clearly categorized beforehand. To address this, training data were generated through the following procedure: first, a portion of the orthomosaic was cropped to include only areas where land-cover features could be clearly distinguished. Subsequently, polygons were manually delineated in QGIS, and land-cover labels were assigned to each polygon. This process produced labeled images with the seven land-cover classes listed in Table 2.

Table 2: Classification of land-cover labels

Label	Class name
0	Ground
1	Birch canopy
2	Grass
3	Japanese pampas grass
4	Non-vegetation objects (e.g., marker poles)
5	Birch trunk
6	Non-birch canopy

From the multispectral and labeled images, VI values were computed for all possible combinations of Equation (2). To evaluate the separability of land-cover classes based on the calculated VIs, the **Fisher Discriminant Ratio (FDR)** was employed. FDR quantifies the ratio between inter-class variance and intra-class variance, and is defined as:

$$FDR = \frac{\sum_{i}^{K-1} n_i(\mu_i - \mu)^2}{\sum_{i=0}^{K-1} n_i \sigma_i^2} \qquad (3)$$

where K denotes the number of classes (7), $n_i$the number of pixels in class i, μ_i the mean VI value of class i, σ_i^2 the variance within class i, and μ the overall mean VI value. FDR, and related approaches such as Linear Discriminant Analysis (LDA), are widely used in remote sensing and other fields for feature selection and classification performance assessment [8].

In this study, the numerator of the FDR represents the between-class variance, which indicates how far apart the mean VI values are among pixel groups belonging to different vegetation classes. A larger difference in the mean values implies a higher separability between different classes. Conversely, the denominator corresponds to the within-class variance**,** which reflects the variability of VI values among pixels belonging to the same class. A smaller variance suggests that the pixels within a given class share more similar characteristics. Therefore, a larger FDR value implies that the VI can distinguish the vegetation classes more clearly, and thus its classification performance is evaluated as higher. In this study, the VI that maximized the FDR was identified as the optimal index.

In the exhaustive search of the coefficients a, …, j in equation (2), the following constraints were applied:

1. Formulas in which all coefficients of the numerator and denominator are sign-reversed (e.g., (A-B)/(A+B) and (B-A)/(B+A)) yield the same vegetation index; therefore, such duplicates were eliminated.
2. To ensure that the spectral characteristics most relevant to vegetation, namely the RedEdge and NIR bands, were sufficiently utilized, an additional condition was imposed such that at least one of the corresponding coefficients (d, e, i, j) in both the numerator and denominator must be nonzero [9].

3 Results and Discussions

3.1 Construction of 3D Models Using SfM

Capture screens of the 3D models for each area, generated using the SfM method based on images taken by the Mavic drone, are shown in Figures 3a and 3b. Although the 3D models created by SfM reasonably reproduce the overall appearance of the real scenes when viewed from a distance, distortions and incomplete representations of tree and leaf structures were frequently observed.

Figure 3a: Capture screens of 3D model of Area A generated by SfM

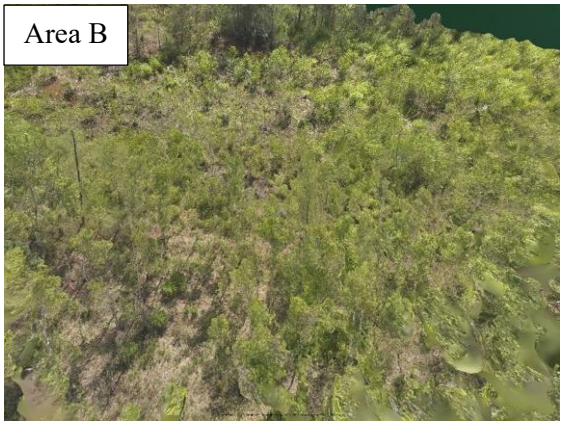

Figure 3b: Capture screens of 3D model of Area B generated by SfM

Capture images of orthomosaics generated using images taken by the Phantom drone are shown in Figures 4a and 4b.

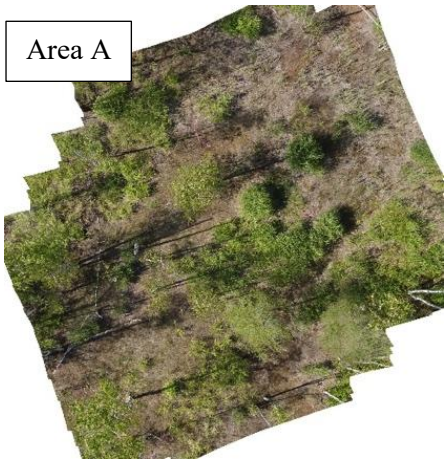

Figure 4a: Orthomosaic of Area A generated by SfM

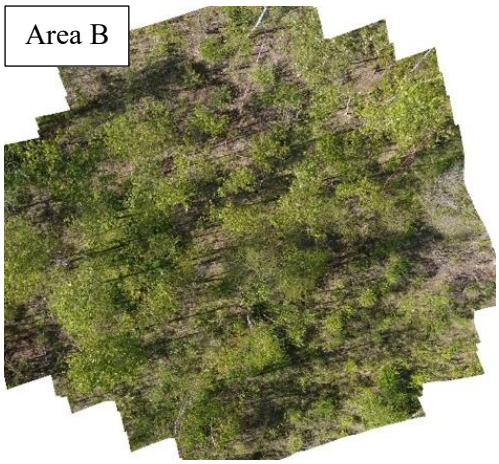

Figure 4b: Orthomosaic of Area B generated by SfM

3.2 Rendering of 3D Models Using 3DGS

Photorealistic renderings were performed using 3D Gaussian Splatting (3DGS) based on the SfM results. Capture screens of the renderings are shown in Figures 5a and 5b. Rendering each area required approximately 1.5 hours. Compared to the 3D models generated by SfM, the 3DGS renderings demonstrated higher fidelity in the representation of trees and leaves, closely approximating their real-world textures.

Figure 5a: Capture screen of the 3D image of Area A generated by 3DGS

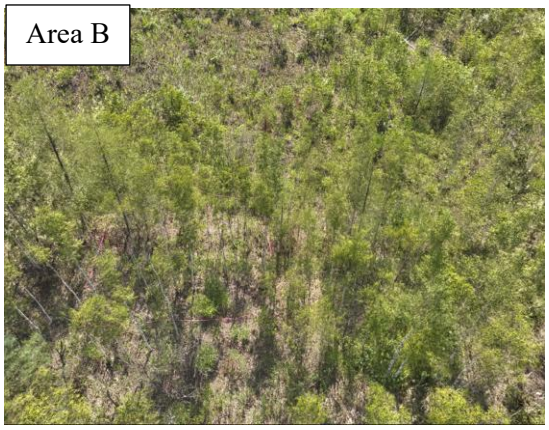

Figure 5b: Capture screen of the 3D image of Area B generated by 3DGS

3.3 Exploration Results of Vegetation Indices

Through the search of Equation (2) and the results of FDR, the following equation was obtained for Area A.

$$\frac{Blue - Green - RedEdge}{Green + Red + RedEdge} \quad (4)$$

Since the color distribution of the colormap was inverted compared to that of NDVI, the sign of the equation was reversed, resulting in:

$$\frac{-Blue + Green + RedEdge}{Green + Red + RedEdge} \quad (4')$$

The FDR value for Equation (4') is identical to that of Equation (4).

Similarly, for Area B, the following equation was obtained.

$$\frac{Blue - Green + Red - NIR}{-Blue - Green + Red - NIR} \quad (5)$$

The index for Area A is defined as the Sparse Vegetation Index (SVI), whereas the index for Area B is defined as the Dense Vegetation Index (DVI). Figures 6 and 7 show, for each area, the RGB image (a), the colormap generated using SVI or DVI (b), and, for comparison, the colormap generated using NDVI (c).

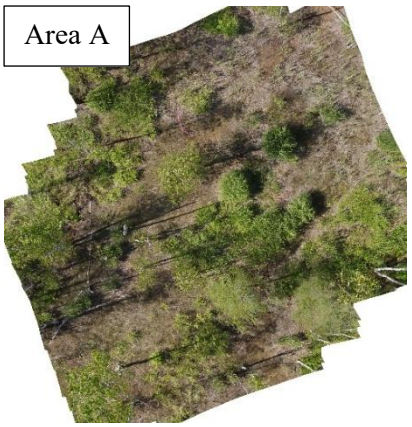

Figure 6a: Orthomosaic of Area A

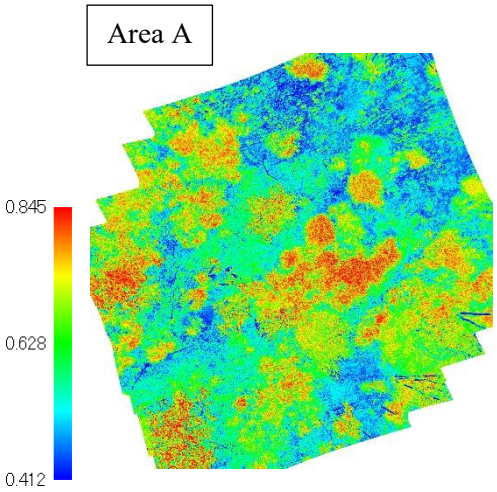

Figure 6b: Colormap of Area A generated using SVI

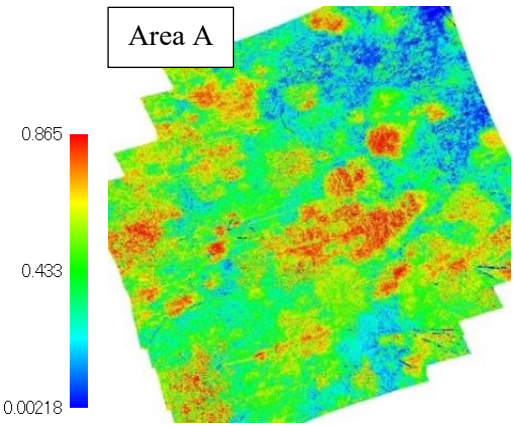

Figure 6c: Colormap of Area A generated using NDVI

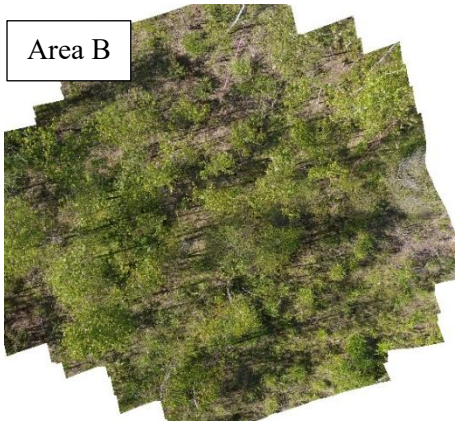

Figure 7a: Orthomosaic of Area

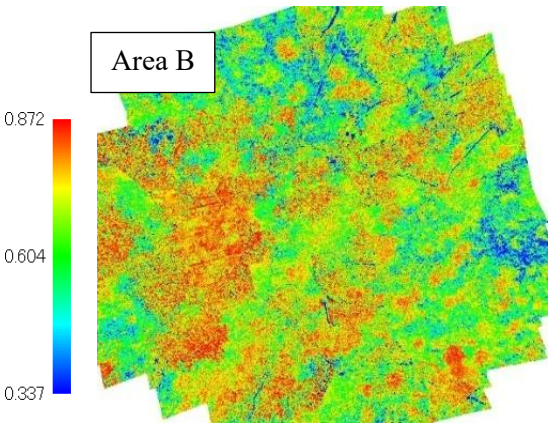

Figure 7b: Colormap of Area B generated using DVI

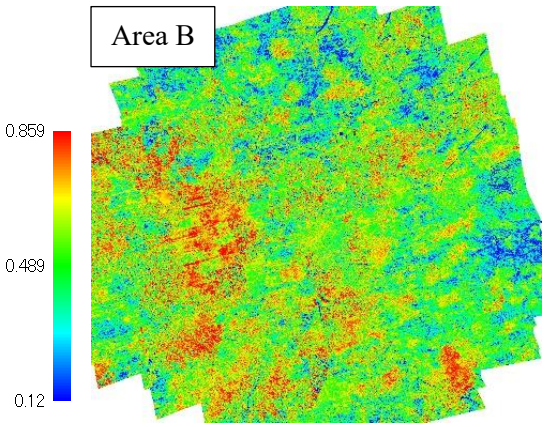

Figure 7c: Colormap of Area B generated using NDVI

In this colormap, a heatmap ranging from red (high) to green (medium) to blue (low) was applied according to the computed index values, with a legend displayed on the left of each figure. In Area A, as shown in Figure 8, comparison between the orthomosaic and the NDVI colormap revealed that some shadowed regions were displayed in red in NDVI, resulting in misclassification of shadows as vegetation. In contrast, the corresponding regions in the SVI colormap did not exhibit such misclassification. This indicates that SVI provides higher accuracy in vegetation discrimination than NDVI in Area A.

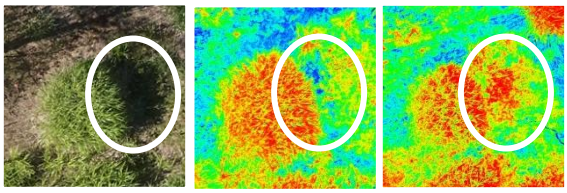

Figure 8: Comparison of shadow areas in Area A

In Area B, the DVI colormap displayed a greater extent of red areas than NDVI, and comparison with the orthomosaic confirmed that these regions corresponded closely to the actual vegetation distribution. NDVI, however, failed to represent some vegetated areas in red, resulting in underestimation of canopy coverage in certain locations. These observations suggest that DVI more accurately reflects vegetation distribution than NDVI in Area B.

Overall, the optimized vegetation indices developed in this study have the potential to visually represent the spatial distribution of specific vegetation more clearly than NDVI, demonstrating their effectiveness as site-specific tools for precise mapping that accounts for regional vegetation characteristics. Nevertheless, several limitations remain. The optimized VI was derived based on training data created by manually labeling polygons in specific trimmed areas, so its applicability is inherently limited. Therefore, the VI obtained from a restricted area cannot be assumed to be universally applicable to the entire study region. Additionally, manual labeling of training data may include human errors. Addressing these limitations will require further investigation.

4 Conclusions

In this study, we constructed 3D models of the abandoned X mine in Hokkaido using SfM techniques based on drone aerial imagery. The resulting 3D models demonstrated a certain level of realism when viewed from distant perspectives; however, distortions were observed in the depiction of tree canopies and herbaceous vegetation at close range, highlighting limitations in horizontal visibility.

Future work should systematically investigate optimal imaging conditions—such as flight altitude, speed, and camera angles—to enable more accurate three-dimensional reconstruction. Furthermore, photorealistic renderings were performed using 3DGS based on the camera alignment information obtained from SfM. Compared to conventional SfM-based models, the 3DGS renderings achieved higher resolution and greater photorealism, demonstrating their effectiveness as a visualization tool for future digital twin construction.

In addition, a novel vegetation index was developed using multispectral orthomosaic images. A full search of formulas combining reflectance from five bands (Blue, Green, Red, RedEdge, and NIR) yielded the optimized indices SVI and DVI, with FDR used to evaluate and maximize discriminative ability between vegetation classes. Unlike the conventional NDVI, which relies solely on the NIR and Red bands, these new indices integrate information from the Blue, Green, and RedEdge bands, allowing them to capture a broader range of spectral features. Compared with NDVI, SVI more accurately distinguished vegetated areas in shadowed regions, avoiding misclassification observed in NDVI, while DVI better captured the actual spatial extent of dense tree canopies. Therefore, the proposed indices have the potential to serve as highly effective vegetation discrimination tools with both enhanced visibility and semantic interpretability.

Overall, the results demonstrate the effectiveness of the proposed methods for high-precision 3D visualization of tailing sites in abandoned mines and for spatial assessment of vegetation conditions using optimized, site-specific vegetation indices. These outcomes provide a technological foundation that could contribute to environmental monitoring and restoration assessment, ultimately supporting the realization of nature-positive initiatives in the future.

References

[1] 環境省, “令和6年版　環境・循環型社会・生物多様性白書　第1部第2章第2節 自然再興（ネイチャーポジティブ）,” 2024. [Online]. Available:https://www.env.go.jp/policy/hakusyo/r06/html/hj24010202.html#n1_2_2. [Accessed: Aug. 1, 2025].

[2] P. Nobahar, C. Xu, P. Dowd, and R. S. Faradonbeh, “Exploring digital twin systems in mining operations: A review,” *Green and Smart Mining Engineering*, vol. 1, no. 4, pp. 474–492, Dec. 2024, doi: 10.1016/j.gsme.2024.09.003.

[3] A. Sharma, E. Kosasih, J. Zhang, A. Brintrup, and A. Calinescu, “Digital Twins: State of the art theory and practice, challenges, and open research questions,” *J. Ind. Inf. Integr.*, doi: 10.1016/j.jii.2022.100383.

[4] S. Huang, L. Tang, J. P. Hupy, Y. Wang, and G. Shao, “A commentary review on the use of normalized difference vegetation index (NDVI) in the era of popular remote sensing,” *ISPRS J. Photogramm. Remote Sens.*, vol. 172, pp. 109–120, Feb. 2021, doi: 10.1007/s11676-020-01155-1.

[5] S. Jiang, C. Jiang, and W. Jiang, “Efficient structure from motion for large-scale UAV images: A review and a comparison of SfM tools,” *ISPRS J. Photogramm. Remote Sens.*, vol. 167, pp. 116–134, Sep. 2020, doi: 10.1016/j.isprsjprs.2020.04.016.

[6] T. Wu et al., “Recent Advances in 3D Gaussian Splatting,” *Vis. Comput.*, doi: 10.1007/s41095-024-0436-y.

[7] 阿部純 他, “岩盤状態の判定に向けた可視化指標開発の検討,” *資源・素材講演集*, vol. 10, no. 2, 2023.

[8] C. Lv et al., “A Classification Feature Optimization Method for Remote Sensing Imagery Based on Fisher Score and mRMR,” *Appl. Sci.*, vol. 12, no. 17, Sep. 2022, doi: 10.3390/app12178845.

[9] Q. Xie et al., “Vegetation Indices Combining the Red and Red-Edge Spectral Information for Leaf Area Index Retrieval,” *IEEE J. Sel. Top. Appl. Earth Obs. Remote Sens.*, vol. 11, no. 5, pp. 1482–1492, May 2018, doi: 10.1109/JSTARS.2018.2813281.